



Semi-empirical estimates of stratospheric circulation and the lifetimes of chlorofluorocarbons and carbon tetrachloride



Stephen Bourguet¹✉, Kane Stone² & Megan Lickley^{1,3}

Chlorofluorocarbons (CFCs) and carbon tetrachloride (CCl_4) are ozone-depleting substances with high radiative efficiencies; however, uncertainties in their atmospheric lifetimes hinder top-down emission monitoring efforts. Here, we compute the loss, emission, and lifetime of CFC-11, CFC-12, and CCl_4 using their mass balance in the stratosphere. We first infer the strength of the stratospheric overturning circulation using satellite measurements of nitrous oxide; the mass flux at about 18 km is then used to compute the loss of CFC-11, CFC-12, and CCl_4 . We confirm that anomalous surface measurements of CFC-11 from 2013 to 2018 cannot be attributed to variability in stratospheric transport alone, and we infer near-steady CCl_4 emissions since 2013. Atmospheric lifetimes (50, 86, and 41 yr) independent of previous work are also computed using loss rates. These estimates add confidence to emission inversions and projections of the compounds' ozone and climate impacts, and may help detect breaches of the Montreal Protocol.

The continued success of the Montreal Protocol in protecting the ozone layer¹ and averting surface warming^{2,3} requires careful monitoring of ozone-depleting substances (ODSs) in the atmosphere. For example, surface measurements of trichlorofluoromethane (CFC-11) were used to detect production in breach of the Montreal Protocol in 2018^{4,5}, which were halted the following year^{6,7}. Meanwhile, the anticipated return of the ozone layer to pre-1980 levels has been delayed in recent Scientific Assessments of Ozone Depletion (SAODs), partially due to measurements suggesting unexpected yet sustained emissions of carbon tetrachloride (CCl_4)^{8,9}. As emissions have not been entirely from reported sources⁶, emission-driven changes in atmospheric ODS burdens must be teased out from observed net changes. This requires accurate and precise estimates of the compounds' atmospheric lifetimes.

To date, ODS lifetimes have been estimated using chemistry-climate models, surface measurements, or satellite retrievals with temporal or spatial data gaps^{10–15}. These methods require assumptions—that climate models accurately represent the true atmosphere, that emissions of these compounds are known, or that observational biases are negligible—and their estimates vary widely. For example, the differences across the 2-sigma confidence intervals of the commonly used CFC-11 and CCl_4 lifetimes are approximately half of the lifetimes' most likely values (see Table 1)¹⁰.

Consequently, measurement-based conclusions regarding non-compliance with the Montreal Protocol will lack certainty unless the measurements fall outside the range of projections that account for these uncertain lifetimes.

In this paper, we present a semi-empirical method for the calculation of CFC-11, dichlorodifluoromethane (CFC-12), and CCl_4 loss, emissions, and lifetimes. This method is founded on the mass balance of compounds destroyed in the stratosphere, and it is validated using output from the Community Earth System Model Whole Atmosphere Community Climate Model (WACCM)^{16,17} (see Supplementary Methods). We first apply this method to satellite measurements of nitrous oxide (N_2O) to calculate the strength of the stratosphere's overturning circulation. This circulation strength is then used to calculate the mass of CFC-11, CFC-12, and CCl_4 destroyed in the stratosphere from 2005 to 2022. Finally, stratospheric loss rates are used to estimate the emissions and atmospheric lifetimes of these compounds, and our results are compared with previous estimates.

Results

The mass balance of compounds destroyed in the stratosphere
CFCs and CCl_4 are destroyed primarily by photolysis or reaction with atomic oxygen ($\text{O}(^1\text{D})$) in the tropical stratosphere^{10,18}. Although

¹Earth Commons, Georgetown University, Washington, DC, USA. ²Department of Earth, Atmospheric, and Planetary Sciences, Massachusetts Institute of Technology, Cambridge, MA, USA. ³Science, Technology, and International Affairs Program, Georgetown University, Washington, DC, USA.

✉e-mail: stephen.bourguet@georgetown.edu

observations of these compounds in their loss regions are not sufficient to accurately compute their loss rates using photochemistry models^{15,19}. CFC-11, CFC-12, and CCl₄ are all observed up to at least the base of their atmospheric loss regions^{19,20}. As stratospheric transport is driven by a slow overturning circulation^{21–23}, with air rising in the tropics and descending in the mid-latitudes and poles, the ODS concentrations of air parcels both before and after they transit the loss region are captured by observations that span the lower stratosphere. Thus, a mass balance of each compound (X) can be employed at a given level in the lower stratosphere to deduce the compound's loss rate above that height (L_X):

$$\frac{dM_X}{dt} = w([X]_{\text{up}} - [X]_{\text{down}}) - L_X, \quad (1)$$

where M_X is the compound's mass above the height of analysis, w is the overturning mass flux at that height, and $[X]_{\text{up}}$ and $[X]_{\text{down}}$ are mass-flux-weighted mass mixing ratios in the upwelling and downwelling regions. As the surface concentrations of the compounds considered here evolved at rates between -1.5 and 0.3% yr⁻¹ from 2005 to 2023²⁴, while variability in transport altered their spatial distributions in the stratosphere^{25–27}, $\frac{dM_X}{dt}$ is taken to be the sum of trend- and transport-driven changes in M_X (see Methods).

To calculate L_X using equation (1), the overturning mass flux of the lower stratosphere must be known. Previous observationally-derived estimates of stratospheric transport have either been qualitative^{21,22}, confined to a narrow region near the equator^{28,29}, or above our height of interest³⁰. Meanwhile, climate models struggle to reproduce stratospheric transport³¹, and reanalysis circulation strengths vary widely^{30,32–34}. Models also predict a warming-driven acceleration, while tracer observations have been inconclusive despite decades of warming^{25,27,32,33,35–39}, leaving the potential evolution of ODS lifetimes uncertain⁴⁰.

We compute the strength of the overturning circulation of the stratosphere by applying equation (1) to retrievals of N₂O from the Atmospheric Chemistry Experiment Fourier Transform Spectrometer (ACE-FTS) onboard the SCISAT-1 from March 2005 to February 2023⁴¹. (We refer to this time period as 2005–2022 hereafter.) This improves upon previous methods by constraining mass flux with a tracer that is observable (i.e., does not require derivation from other observed tracers), is measured throughout the stratosphere, and has no stratospheric source and a well-understood sink. Unlike CFC-11, CFC-12, and CCl₄, ACE-FTS observations of N₂O have sufficient vertical resolution for its loss to be computed offline with a photochemistry model using seasonal averages^{20,42–45}, as is shown in Fig. 1A–B. In solving equation (1), each variable is averaged over

five years to smooth out interannual variability in stratospheric transport⁴⁶, and potential temperature is used as the vertical coordinate to separate diabatic vertical motion from adiabatic horizontal motion³⁰. The strength of the stratospheric circulation is computed from 400 K to 1100 K (~18 km to 35 km in the tropics), and CFC-11, CFC-12, and CCl₄ loss rates are evaluated at 400 K. This method was validated in WACCM, with a potential high bias in circulation strength in the lower stratosphere that does not impact loss rate calculations (see Supplementary Fig. 1 and Supplementary Table 1).

The strength of the stratospheric overturning circulation from 2005 to 2022 is shown in Fig. 1C. At 400 K, the overturning mass flux was $12.0\text{--}15.7 \times 10^9 \text{ kg s}^{-1}$ (95% CI) for 5-year averages during this period. The circulation strength at 400 K has not been calculated from tracer observations previously; however, we find a circulation strength at 460 K ($5.5\text{--}7.1 \times 10^9 \text{ kg s}^{-1}$) that is weaker than a previous N₂O-derived estimate ($6.3\text{--}7.6 \times 10^9 \text{ kg s}^{-1}$)³⁰. We attribute the difference between these estimates to methodological differences in how N₂O distributions are related to circulation strength. Linz and colleagues³⁰ assumed a relationship between the meridional N₂O gradient and the residence time of air above 460 K⁴⁷, and the mass flux was then computed based on the ratio of mass above 460 K to the approximated residence time. The method presented here employs a mass balance of N₂O itself and thus is not subject to potential biases in the relationship between N₂O gradients and residence time³³.

Loss rates and inferred emissions of CFC-11, CFC-12, and CCl₄

Annual loss rates of CFC-11, CFC-12, and CCl₄ computed using the five-year running-mean overturning mass flux at 400 K are shown in Fig. 2 (solid lines). Following from the decline in the atmospheric burden of these compounds²⁴, their respective loss rates decreased by 16%, 17%, and 25% from the 5-year period centered around 2007 to the period centered around 2020. Loss rates were also modulated by the strength of the overturning circulation at 400 K, which we find decreased by 11% (1-sigma CI: -17% , -4%) from 2007 to 2014 before increasing by 4% (-3% , 12%) through 2022. This net decreasing trend, though insignificant at the 1-sigma confidence level, contrary to climate model projections^{32,35–37}, and sensitive to height (see Fig. 3), would be consistent with the effects of the ozone layer's recovery on stratospheric circulation^{48–50}.

For compounds with lifetimes substantially longer than the mixing timescale of the atmosphere, emissions over a given time period can be computed from the compound's change in atmospheric burden and time-integrated global loss⁵¹:

$$\text{Emissions}_t = (\text{Burden}_{t+1} - \text{Burden}_t) + \text{Global Loss}_t, \quad (2)$$

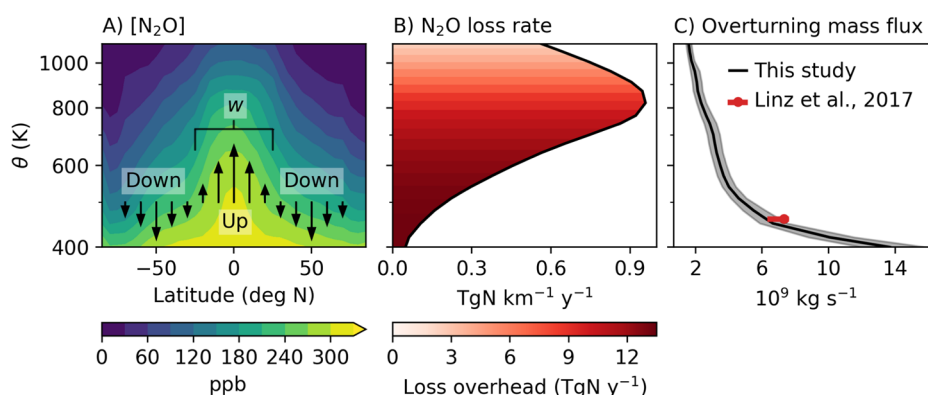


Fig. 1 | Stratospheric N₂O mixing ratios, N₂O loss rate, and overturning circulation. A Zonal mean ACE-FTS N₂O mixing ratios from 2005 to 2022, with arrows denoting approximate areas of upward and downward mass flux. B Time-average N₂O loss rate as a function of height, calculated using seasonal N₂O profiles from 2005 to 2022 and a photochemistry model. Shading denotes the total loss above a given height ($L_{\text{N}_2\text{O}}$ in equation (3)). C The overturning circulation strength

according to the mass balance of N₂O above each isentrope, with a previous observationally-derived strength at 460 K³⁰ included for comparison. The solid line shows the median circulation strength from 2005 to 2022, and the shading denotes the 95% CI of the 5-year average circulation strength when accounting for measurement uncertainty and temporal variability.

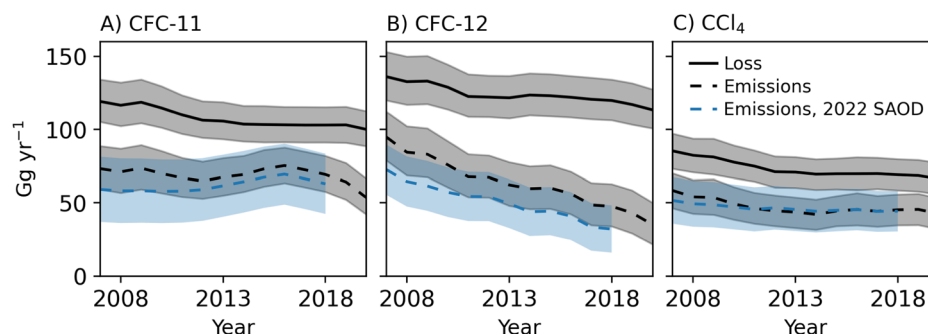


Fig. 2 | CFC-11, CFC-12, and CCl₄ loss and emission. Five-year running averages of (solid lines) loss rates calculated according to the mass balance of each compound above 400 K, (black dashed lines) emissions calculated using aforementioned loss rates and atmospheric burdens estimated from surface measurements, and (blue dashed lines) emissions from the 2022 Scientific Assessment

of Ozone Depletion⁵² for **A** CFC-11, **(B)** CFC-12, and **C** CCl₄. Loss rates are adjusted to account for loss below 400 K (see Methods), with CCl₄ loss further adjusted to include ocean and soil sinks with lifetimes of 124 yr (1-sigma CI: 110, 150 yr) and 375 yr (288, 536 yr), respectively^{52,70,71}. Shading denotes 95% CIs, with the 2022 SAOD uncertainties solely from the compounds' lifetimes.

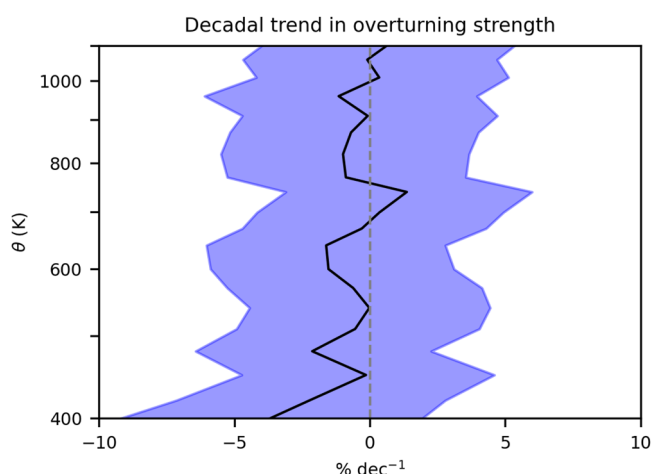


Fig. 3 | The trend in the stratospheric overturning circulation, 2005 to 2022. The decadal trend in the strength of the stratospheric overturning circulation from 400 K to 1100 K (~18 km to 35 km in the tropics) according to linear regressions computed at each height from 2005 to 2022. The black line shows the median trend at each height, and the shading denotes the 1-sigma CI. Best fit trends and their uncertainties were computed for each of the 10,000 samples (see Methods), and each trend was then sampled independently 1000 times to create a distribution of possible trends according to both measurement and statistical uncertainties.

where t is the time period where emissions and loss are being evaluated, and $t + 1$ is the following time period. Atmospheric burdens of CFC-11, CFC-12, and CCl₄ are computed using surface observations from the Advanced Global Atmospheric Gases Experiment (AGAGE)²⁴, and global loss is scaled from stratospheric loss using compound-specific conversion factors (see Methods). Using equation (2), five-year running mean annual emissions are then calculated from 2005 to 2022 (Fig. 2, dashed black lines). Notably, CFC-11 emissions peak in 2016, corroborating the previous detection of unexpected emissions and their subsequent cessation^{4–7}, and CCl₄ emissions were steady at 44 Gg yr^{−1} (95% CI: 34, 55 Gg yr^{−1}) after 2013. This is consistent with previous work highlighting this unexpectedly persistent emission⁸ that has delayed the anticipated recovery of the ozone layer⁹.

Our results suggest that CFC-11 and CFC-12 emissions from 2005 to 2020 were likely greater than those estimated in the 2022 SAOD (Fig. 2, dashed blue lines)⁵², although uncertainties overlap. By using satellite measurements for loss calculations, we also reduce emissions uncertainty relative to the 2022 SAOD and capture transport-driven variability in loss. This approach contrasts with the use of an atmospheric transport model that is informed solely by surface measurements and has loss parameterized

with fixed, uncertain lifetimes^{13,52}. This is most notable for CFC-11, where the 95% CI is reduced from over 40 Gg yr^{−1} to ~25 Gg yr^{−1} for the five-year averages after 2010.

Additionally, we find that the fractional elevation of CFC-11 emissions in 2014–2018 relative to 2008–2012 was likely lower than what was estimated in the 2022 SAOD (7% (1-sigma CI: −4%, 20%) compared to 20%) due to a weakening of the stratospheric circulation that is captured in our analysis. Our estimate still suggests an unexpected emission source, as CFC-11 emissions were expected to decrease over this time in the absence of new production. Following from our 2008–2012 estimate, emissions would have decreased from 70 Gg yr^{−1} (1-sigma CI: 63, 78 Gg yr^{−1}) to 59 Gg yr^{−1} (53, 65 Gg yr^{−1}) from 2010 to 2016, assuming a 3% annual release rate of CFC-11 from reservoirs^{4,6}. Here, we estimate 2014–2018 emissions to be 75 Gg yr^{−1} (69, 82 Gg yr^{−1}), suggesting unexpected emissions of 17 Gg yr^{−1} (9, 24 Gg yr^{−1}). If the 2008–2012 circulation strength is used to calculate 2014–2018 emissions, then inferred emissions in the latter period would be 80 Gg yr^{−1} (73, 87 Gg yr^{−1}). Therefore, the estimated magnitude of unexpected CFC-11 emissions from 2014 to 2018 is lowered by 5 Gg yr^{−1} (−3, 13 Gg yr^{−1}), or 22% (−15%, 57%), when changes to the circulation strength are considered. This confirms that a weakened stratospheric circulation was not the only driver of unexpected CFC-11 measurements; it is likely that an unexpected emission source also contributed.

Narrowed uncertainty in lifetime estimates for CFC-11, CFC-12, and CCl₄

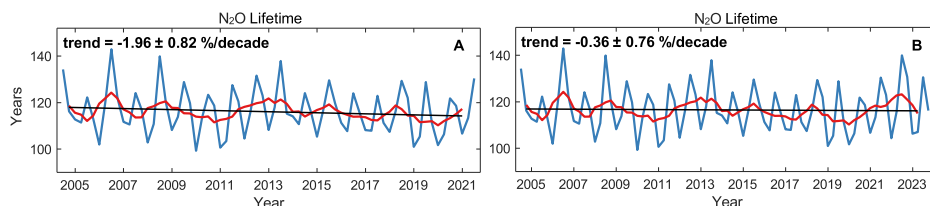
Using loss rates computed with equation (1) and atmospheric burdens derived from AGAGE, we estimate the atmospheric lifetimes of CFC-11, CFC-12, and CCl₄ (Table 1). These lifetimes reflect the average atmospheric decay of these compounds over a five-year period and thus do not capture variability on shorter timescales, such as that driven by the quasi-biennial oscillation. Air parcels that transit the loss region have a spectrum of multi-year stratospheric residence times⁵³, so lifetime variability on shorter timescales should have little impact on surface measurements and emission

Table 1 | Lifetime estimates of CFC-11, CFC-12, and CCl₄ with regard to photochemical removal in the atmosphere (yr) and a comparison with previously published estimates

Compound	Mass balance at 400 K	SPARC
CFC-11	50 (43, 57)	52 (43, 67)
CFC-12	86 (75, 99)	102 (88, 122)
CCl ₄	41 (34, 51)	44 (36, 58)

Values computed in the present study are reported as the mean for 2005 to 2022 with the 95% CI accounting for both statistical and measurement uncertainties (see Methods). Values reported in SPARC account for weighted uncertainties across independent methods, with the uncertainties reported as 2-sigma CIs (see ref.¹⁰ for further details).

Fig. 4 | N₂O lifetime trends. **A** The N₂O lifetime calculated using ACE-FTS N₂O measurements and a photochemistry model from 2004 to 2021 and the corresponding decadal trend. **B** The same as panel A but for years 2004 to 2023. Note the difference in trend based on choice of end-year. Blue lines show the lifetime for each season, while the red lines show the running annual average.



inversions. However, approximately half of the uncertainty presented here reflects longer-term variability in the stratospheric circulation (with the other half reflecting systematic measurement uncertainty). This uncertainty is not fully correlated through time and would not cancel out when comparing emission estimates across time periods. As the atmospheric burdens of these compounds have declined by 1% yr⁻¹ or less since 2005²⁴, these lifetimes are reflective of near-steady state conditions, i.e., periods when emissions are low.

By informing lifetimes with satellite measurements of the lower stratosphere, we estimate narrower uncertainties relative to the 2013 Stratospheric Processes and their Role in Climate (SPARC) report on Lifetimes of Stratospheric Ozone-Depleting Substances, Their Replacements, and Related Species¹⁰. In particular, we find that the highest values within the SPARC most likely ranges are not consistent with observations. The shorter lifetimes computed here imply lower global warming potentials. Notably, the CFC-11 and CFC-12 lifetimes are consistent with those found by an independent Bayesian analysis of CFC production, emissions, and lifetimes (medians and 95% CIs of 49.1 yr (44.1, 54.6 yr) and 84.7 yr (76.7, 95.5 yr)), which also did not assume that emissions were known but was constrained using surface measurements⁵⁴. As parameterized lifetimes are inverse to emissions in atmospheric transport models¹³, our results suggest that true emissions were at the high end of previous estimates. This is consistent with the relative magnitudes of the emission estimates in Fig. 2: 2022 SAOD estimates were computed with SPARC lifetimes, and their loss and emission uncertainties encompass lower values than those calculated here.

Emissions can be estimated prior to 2005 using the lifetimes presented here after accounting for deviations from steady state¹⁰. Increased confidence around historical emission estimates allow for better constraints on the mass of CFC-11 and CFC-12 stored in aging equipment⁵⁴, which can update expectations for future emissions from these sources and inform future efforts to recover stored compounds. A reduction in lifetime uncertainty also allows for more precise projections of future atmospheric burdens⁵¹. These improvements could reduce the lead time required to detect a breach in the Montreal Protocol and refine projections of future ozone depletion and surface warming driven by these compounds.

Discussion

This work presents a semi-empirical method to calculate the strength of the stratospheric overturning circulation, and with that, the loss, emissions, and lifetimes of compounds destroyed in the stratosphere. This adds confidence to established emission inversion methods (e.g., ref. 13) by informing loss rates with satellite measurements of ODSs. These loss rates also yield lifetime estimates that are independent of previous work¹⁰ while minimizing assumptions regarding atmospheric transport and surface emissions. Although our method does not account for diabatic diffusion⁵⁵, which would dampen concentration gradients in the stratosphere, our WACCM validation suggests that this effect is small and compensated for in lifetime estimates (see Supplementary Methods). Nonetheless, increased measurement frequency of the lower stratosphere—especially in the tropics—could reduce the sampling uncertainty of upwelling and downwelling fluxes for all compounds and increase confidence in N₂O photochemical loss rate calculations.

The circulation strength derived here from N₂O measurements suggests a possible deceleration at 400 K from 2005 to 2022, which is consistent with the impacts of a recovering ozone layer^{48–50}. However, a deceleration is

in disagreement with climate model projections^{32,35–37} and a recent analysis of N₂O observations from 2004 to 2021²⁷, although an extension of that method through 2023 yields closer agreement with the results presented here (see Fig. 4). If this deceleration is part of an ozone healing-driven trend, then the declining atmospheric burdens of CFC and CCl₄ may act as a negative feedback on their loss rates—or a positive feedback on their lifetimes. This contrasts the negative feedback on CFC lifetimes that has been previously proposed, which would take effect if the surface warming driven by these gases were to accelerate the stratospheric circulation⁴⁰. As the trend shown here is not significant at the 1-sigma confidence level, we present this positive feedback with caution; nonetheless, future model validation and emission inversion efforts should consider its existence. Continued monitoring of stratospheric N₂O and ODS distributions is needed to refine stratospheric transport in models and reanalyses, constrain lifetimes, and maintain compliance with the Montreal Protocol in a changing climate.

Methods

This work aims to compute the loss of CFC-11, CFC-12, and CCl₄ using the difference in their masses flowing into and out of their stratospheric loss regions. To do so, we first compute the strength of the stratospheric overturning circulation by rearranging Eq. (1) and applying it to ACE-FTS retrievals of N₂O:

$$w = ([N_2O]_{up} - [N_2O]_{down})^{-1} \left(\frac{dM_{N_2O}}{dt} + L_{N_2O} \right). \quad (3)$$

As noted in the Main Text, ACE-FTS measurements of N₂O have sufficient spatial and temporal coverage for the evaluation of Eq. (3) on seasonal timescales, while measurements of CFC-11, CFC-12, and CCl₄ do not. The computed overturning mass flux, w , is then entered into Eq. (1), and the loss of CFC-11, CFC-12, and CCl₄ are solved for as:

$$L_X = ([N_2O]_{up} - [N_2O]_{down})^{-1} \left(\frac{dM_{N_2O}}{dt} + L_{N_2O} \right) ([X]_{up} - [X]_{down}) - \frac{dM_X}{dt}. \quad (4)$$

Below, we describe the observational data used in this study and the calculation method for each term on the right side of Eq. (4). We then describe the calculation of CFC-11, CFC-12, and CCl₄ lifetimes and their uncertainties.

ACE-FTS retrievals

N₂O, CFC-11, CFC-12, CCl₄, and temperature profiles were obtained from version 5.2 of the Atmospheric Chemistry Experiment Fourier Transform Spectrometer (ACE-FTS) retrievals⁴¹. The relatively high abundance of N₂O allows for its measurement by ACE-FTS up to 80 km, while CFC-11, CFC-12, and CCl₄ mixing ratios fall below the detection limit of ACE-FTS in the middle stratosphere. These data were supplied on altitude levels with 1.0 km vertical spacing and were interpolated onto potential temperature surfaces using colocated pressures from the European Centre for Medium-Range Weather Forecasts Reanalysis v5 (ERA5)⁵⁶. Isentropic levels were then chosen based on potential temperatures in the tropics, with spacing increasing from 20 K at 400 K to 50 K at 1100 K.

Data for each season (MAM, JJA, SON, and DJF, with DJF used for the JF year) were averaged in bins centered at 85°S to 85°N with 5° spacing. To

avoid unphysical retrievals, values were removed prior to binning if they: 1) were less than 0, 2) had a reported statistical fitting error less than 0, or 3) were greater than 1.05 times the maximum Advanced Global Atmospheric Gases Experiment (AGAGE)²⁴ surface mixing ratio from the year prior to the retrieval. Following the recommended procedure of the ACE-FTS data usage guide, values in each bin were detrended, the median absolute deviations (MADs) of the detrended time series were calculated, and all values greater than three MADs from the median were removed. The 5-year running mean average of the remaining values in each seasonal bin were then taken, with each five-year window detrended to prevent bias in the case of temporal data gaps. Polar data were filled in with the nearest value when missing; the mass at the poles is small, so the possible bias introduced by this extrapolation is minimal. Data were otherwise available in each five-year bin for each season from MAM 2005 through DJF 2023.

ACE-FTS reported statistical fitting errors were generally less than 1.5% of the measured value outside of the tropics and less than 3% within the tropics. To account for this uncertainty, each retrieval was independently sampled 10,000 times from a normal distribution with a mean equal to the reported measurement and standard deviation equal to the reported uncertainty. An additional 3% uncertainty was included after computing seasonal profiles to account for potential systematic biases^{57–59}. The overturning circulation strength, loss, emissions, and lifetimes were then computed for each of the 10,000 sets of retrievals.

Mass-flux weighting of $[X]_{up}$ and $[X]_{down}$

Mass-flux weighting was used to capture the average concentrations of N_2O , CFC-11, CFC-12, and CCl_4 upwelling and downwelling through a given isentrope ($[X]_{up}$ and $[X]_{down}$)⁶⁰. These relative weights are used to approximate the meridional structure of upwelling and downwelling on a given isentrope to $[X]$ without assuming a circulation strength. This was done according to the following equations:

$$[X]_{up} = \left(\int \sigma \dot{\theta} dA_{up} \right)^{-1} \int [X] \sigma \dot{\theta} dA_{up}, \quad (5)$$

$$[X]_{down} = \left(\int \sigma \dot{\theta} dA_{down} \right)^{-1} \int [X] \sigma \dot{\theta} dA_{down}, \quad (6)$$

where σ is the isentropic density ($-g^{-1} \frac{dp}{d\theta}$), $\dot{\theta}$ is the diabatic heating rate (i.e., potential temperature tendency), and A_{up} and A_{down} are the regions of heating (upwelling) and cooling (downwelling), respectively. σ , $\dot{\theta}$, A_{up} , and A_{down} were computed from monthly mean, zonal mean reanalysis pressures, temperatures, and temperature tendencies. Sets of these variables were independently sampled from two reanalyses to increase robustness (ERA5 and the Modern-Era Retrospective analysis for Research and Applications, Version 2 (MERRA-2)⁶¹), with an equal number of samples drawn from each reanalysis. As A_{up} and A_{down} closely agree between the reanalyses, lifetimes vary by less than 1% if only one reanalysis is used. All variables were binned by season from MAM 2005 through DJF 2023 and were interpolated to 1° meridional spacing to ensure that the upwelling and downwelling regions were properly delineated.

Seasonal weighting

The strength of the stratospheric overturning circulation and the meridional distribution of tracers vary seasonally^{62,63}, so the mass flux of each compound was separated into seasonal components to capture potential covariance between these terms. To do so, we computed $[X]_{up}$ and $[X]_{down}$ as the weighted average of each season (s):

$$[X]_{up} = \sum_s f_s [X]_{up,s}, \quad (7)$$

$$[X]_{down} = \sum_s f_s [X]_{down,s}. \quad (8)$$

The seasonal weights (f_s) were determined by the relative strength of the diabatic circulation during each season in reanalyses (D)⁶⁰:

$$D_{up,s} = \int \sigma_s \dot{\theta}_s dA_{up,s}, \quad (9)$$

$$D_{down,s} = \int \sigma_s \dot{\theta}_s dA_{down,s}, \quad (10)$$

$$D_s = \frac{D_{up,s} + D_{down,s}}{2}, \quad (11)$$

$$f_s = D_s \left(\sum_s D_s \right)^{-1}. \quad (12)$$

Though this introduced dependence on reanalysis upwelling profiles through their seasonality, w and the corresponding CFC and CCl_4 lifetimes vary by less than 1% if the weights are all set to 0.25 (i.e., seasonality is ignored).

Time tendency of stratospheric burden, $\frac{dM_X}{dt}$

The mass of a tracer above a given height in the atmosphere may vary due to changes in its total atmospheric burden (i.e., imbalance between emissions and loss, see Eq. (2)) or due to changes in atmospheric transport. Therefore, we assumed:

$$\frac{dM_X}{dt} = \frac{dM_{X,B}}{dt} + \frac{dM_{X,tran}}{dt}, \quad (13)$$

where $\frac{dM_{X,B}}{dt}$ and $\frac{dM_{X,tran}}{dt}$ are the change in M_X driven by the changes in total atmospheric burden and the transport, respectively. As the atmospheric burdens of N_2O , CFC-11, CFC-12, and CCl_4 changed from 2005 to 2023²⁴, $\frac{dM_{X,B}}{dt}$ was non-zero for each compound during the study period. $\frac{dM_{X,tran}}{dt}$ may have varied^{25–27}, and we assumed that the impact of atmospheric transport on the spatial distributions of N_2O , CFC-11, CFC-12, and CCl_4 was related across compounds⁶⁴.

The change in mass of N_2O above a given isentrope ($\frac{dM_{N_2O}}{dt}$) was computed using ACE-FTS N_2O and colocated ERA5 pressures. The forward difference was used to maintain consistency with the treatment of global burdens (equation (2)). ACE-FTS cannot measure CFC-11, CFC-12, and CCl_4 throughout the stratosphere; therefore, we estimated $\frac{dM_{X,B}}{dt}$ and $\frac{dM_{X,tran}}{dt}$ for each compound and summed the two. To do so, we first estimated the masses of CFC-11, CFC-12, and CCl_4 above 400 K using an assumed relationship between those masses and the mass of N_2O above 400 K:

$$M_X = \frac{[X]_{surf,AGAGE}}{[N_2O]_{surf,AGAGE}} \left(\frac{[X]_{surf,WACCM}}{[N_2O]_{surf,WACCM}} \right)^{-1} \frac{M_{X,WACCM}}{M_{N_2O,WACCM}} M_{N_2O,ACE}, \quad (14)$$

where the ratio of AGAGE surface measurements was used to account for the relative abundance of compound X to N_2O at entry to the stratosphere, and output from the Community Earth System Model version 2 run with the Whole Atmosphere Community Climate Model version 6 (WACCM) was used to account for differences in the stratospheric distributions across compounds. The mass of compounds above 400 K in WACCM ($\frac{M_{X,WACCM}}{M_{N_2O,WACCM}}$) was normalized by model surface concentrations ($\frac{[X]_{surf,WACCM}}{[N_2O]_{surf,WACCM}}$) to account for differences in the tropospheric burden between the model and observations. $\frac{dM_{X,B}}{dt}$ was then calculated based on the change in surface concentration of each compound, lagged by two years to account for the mixing time of surface perturbations⁶⁵:

$$\frac{dM_{X,B,t}}{dt} = \frac{([X]_{surf,AGAGE,t-1} - [X]_{surf,AGAGE,t-2})}{[X]_{surf,AGAGE,t-2}} M_{X,t}. \quad (15)$$

$\frac{dM_{N_2O,tran}}{dt}$ was isolated from $\frac{dM_{N_2O}}{dt}$ using Eqs. (13) and (15), and $\frac{dM_{X,tran}}{dt}$ was calculated as:

$$\frac{dM_{X,tran}}{dt} = \frac{dM_{N_2O,tran}}{dt} \frac{M_X}{M_{N_2O}}. \quad (16)$$

Equations (14)–(16) assume that the relationships between the atmospheric distributions of N_2O and those of CFC-11, CFC-12, and CCl_4 are well represented in WACCM, which has been shown in previous work^{17,66} (see Supplementary Methods for further detail on WACCM output). In addition, these compounds' lifetimes in WACCM are within the uncertainties of those computed here, implying comparable stratospheric distributions (see Table 1 and Supplementary Table 1). We also assumed that trends in stratospheric burdens follow trends in tropospheric burdens. Observations show that lower stratospheric trends agree with surface trends²⁰, but trends may differ higher in the stratosphere. The mass of the atmosphere and the mixing ratios of N_2O , CFC-11, CFC-12, and CCl_4 decrease with height, so we assumed errors resulting from disagreements with surface trends were small. We note that $\frac{dM_X}{dt}$ is $\sim 0.03L_X$ for each compound, suggesting that this term is a small source of uncertainty in equation (1).

Loss rates and lifetime of N_2O , L_{N_2O}

Atmospheric photolytic loss of N_2O was calculated semi-empirically using the TUV 5.4 photochemistry model with the 2-stream pseudo-spherical option. The model computes loss by photolysis and reaction with the $O(^1D)$ radical at 1 km height levels^{42,43}. Observations of N_2O , temperature, and pressure from ACE-FTS and O_3 from the Aura Microwave Limb Sounder (MLS)⁶⁷ were used. (ACE-FTS O_3 has a known high bias above 20 km⁶⁸, while MLS O_3 measurements are well validated and were assumed to have no uncertainty^{45,68}.) 3-monthly (seasonal) and 5° zonal (87.5°S–87.5°N) averages were used. ACE-FTS pressure data were corrected below 30 km to ERA5 to account for a small step change in ACE-FTS pressure after 2015 in the lower stratospheric and upper tropospheric tropical region. To reduce computational costs, photolysis rates were calculated for each hour of the 16th day of each month for each latitude bin using the corresponding seasonal O_3 , temperature, and pressure profiles and then averaged into seasonal photolysis rates. Comparison of this method with photolysis rates when using every day in a month produces only minor differences in key N_2O loss regions (less than -0.5%). $O(^1D)$ concentrations were calculated assuming photochemical equilibrium using photolytic rates of O_3 calculated using TUV 5.4 as above and ACE-FTS reported N_2 and O_2 mixing ratios using Jet Propulsion Laboratory recommended kinetics (<https://jpldataeval.jpl.nasa.gov/pdf/NASA-JPL%20Evaluation%2019-5.pdf>; last accessed February 25, 2025).

L_{N_2O} was calculated by summing the loss above each height, which was then interpolated onto isentropic levels using the latitude-weighted potential temperature of each altitude level from 45°S to 45°N. (Approximately 90% of annual average N_2O loss occurs within this latitude range⁴⁵; stratospheric circulation estimates vary by less than 1% if 60°S–60°N or 30°S–30°N are used.) A 4.5% 1-sigma uncertainty was assumed according to uncertainties in ACE-FTS N_2O measurements, photolysis rates, kinetics, and the potential error associated with our temporal sampling of monthly loss rates.

Lifetimes of CFC-11, CFC-12, and CCl_4

Atmospheric lifetimes (τ_X) were then calculated from loss rates according to the following relationship:

$$\tau_X = R_X L_X^{-1} B_X, \quad (17)$$

where R_X is the ratio between stratospheric loss and total atmospheric loss for compound X , and B_X is the atmospheric burden. R_X values were computed using loss rates output by three configurations of WACCM; the loss above 400 K and the total atmospheric loss were summed for each model

and ratios were taken. R_X was sampled from normal distributions centered at 0.92, 0.98, and 0.88 for CFC-11, CFC-12, and CCl_4 , respectively, with standard deviations of 0.01, 0.005, and 0.01 that reflect interannual variability and the spread across model configurations. R_X values are slightly smaller than previously reported ratios between stratospheric and total atmospheric loss¹⁰, as R_X accounts for the loss that occurs between the tropopause and 400 K. B_X was computed from surface mixing ratios as $B_X = [X]_{surf} M_{atm} F_X^{-1}$, where $[X]_{surf}$ is the AGAGE global mean surface mass mixing ratio²⁴, M_{atm} is the mass of the atmosphere (5.15×10^{18} kg), and F_X is a WACCM-informed factor that accounts for the elevation of surface mixing ratios relative to global mean mixing ratios (1.07, 1.05, 1.08 for CFC-11, CFC-12, for CCl_4 , respectively, with standard deviations of 0.025; F_{CFC-11} is consistent with that used in past work⁵¹). $[X]_{surf}$ was assigned systematic 1-sigma uncertainties of 1% for CFC-11 and CFC-12 and 2% for CCl_4 .

Uncertainties in τ_X were computed through Monte Carlo sampling. As described above, each ACE-FTS measurement was sampled 10,000 times according to its reported uncertainty. Each time series (L_{N_2O} and $[X]_{surf}$) was sampled with full temporal correlation (i.e., all years were sampled at the same percentile of the variable's distribution), and constants (R_X and F_X) were sampled 10,000 times from their respective distributions. The 2.5–97.5% CIs were then taken from the 140,000 lifetime estimates (each of the 10,000 samples consisted of 14 five-year averages from 2005 to 2022).

Data availability

AGAGE surface measurements are available at <http://agage.mit.edu/data/agage-data> (last accessed February 25, 2025). ACE-FTS retrievals are available upon registration at https://database.scisat.ca/level2/ace_v5.2/ (last accessed February 25, 2025). ERA5 pressures, temperatures, and temperature tendencies due to parameterizations can be accessed through Copernicus Climate Change Service (<https://apps.ecmwf.int/data-catalogues/era5/?class=ea>, last accessed February 25, 2025). MERRA-2 pressures, temperatures, and temperature tendencies (M2TMNPTDT) and MLS O_3 measurements can be obtained from the Goddard Earth Sciences Data and Information Services Center (<https://disc.gsfc.nasa.gov/>) (last accessed February 25, 2025). AGAGE data and processed ACE-FTS, ERA5, MERRA-2, and WACCM data required for analysis in the Main Text and Supplementary Information are available on Zenodo (<https://doi.org/10.5281/zenodo.15652978>)⁶⁹.

Code availability

Jupyter notebooks used to process, analyze, and plot data for the Main Text and Supplementary Information are available on Zenodo (<https://doi.org/10.5281/zenodo.15652978>)⁶⁹.

Received: 25 March 2025; Accepted: 18 June 2025;

Published online: 05 July 2025

References

- Newman, P. A. et al. What would have happened to the ozone layer if chlorofluorocarbons (CFCs) had not been regulated? *Atmos. Chem. Phys.* **9**, 2113–2128 (2009).
- Montzka, S., Dlugokencky, E. & Butler, J. Non-CO2 greenhouse gases and climate change. *Nature* **476**, 43–50 (2011).
- Goyal, R. et al. Reduction in surface climate change achieved by the 1987 Montreal Protocol. *Environ. Res. Lett.* **14**, 124041 (2019).
- Montzka, S. A. et al. An unexpected and persistent increase in global emissions of ozone-depleting CFC-11. *Nature* **557**, 413–417 (2018).
- Rigby, M. et al. Increase in CFC-11 emissions from eastern China based on atmospheric observations. *Nature* **569**, 546–550 (2019).
- Montzka, S. A. et al. A decline in global CFC-11 emissions during 2018–2019. *Nature* **590**, 428–432 (2021).
- Park, S. et al. A decline in emissions of CFC-11 and related chemicals from eastern China. *Nature* **590**, 433–437 (2021).

8. Liang, Q., Newman, P. A. & Reimann, S. The Mystery of Carbon Tetrachloride SPARC Report No. 7 (SPARC, 2016); www.sparc-climate.org/publications/sparc-reports/sparc-report-no7.
9. Lickley, M. J., Daniel, J. S., McBride, L. A., Salawitch, R. J. & Velders, G. J. M. The return to 1980 stratospheric halogen levels: a moving target in ozone assessments from 2006 to 2022. *Atmos. Chem. Phys.* **24**, 13081–13099 (2024).
10. Ko, M. K. W., Newman, P. A., Reimann, S. & Strahan, S. E. Lifetimes of stratospheric ozone-depleting substances, their replacements, and related species. SPARC Report No. 6 (SPARC, 2013); <http://www.sparc-climate.org/publications/sparc-reports/>.
11. Chipperfield, M. P. et al. Multimodel estimates of atmospheric lifetimes of long-lived ozone-depleting substances: present and future. *J. Geophys. Res.* **119**, 2555–2573 (2014).
12. Liang, Q. et al. Constraining the carbon tetrachloride (CCl₄) budget using its global trend and inter-hemispheric gradient. *Geophys. Res. Lett.* **41**, 5307–5315 (2014).
13. Rigby, M. et al. Re-evaluation of the lifetimes of the major CFCs and CH₃CCl₃ using atmospheric trends. *Atmos. Chem. Phys.* **13**, 2691–2702 (2013).
14. Minschwaner, K. & Siskind, D. E. A new calculation of nitric oxide photolysis in the stratosphere, mesosphere, and lower thermosphere. *J. Geophys. Res.* **98**, 20401–20412 (1993).
15. Minschwaner, K. et al. Stratospheric loss and atmospheric lifetimes of CFC-11 and CFC-12 derived from satellite observations. *Atmos. Chem. Phys.* **13**, 4253–4263 (2013).
16. Marsh, D. R. et al. Climate change from 1850 to 2005 simulated in CESM1(WACCM). *J. Clim.* **26**, 7372–7391 (2013).
17. Gettelman, A. et al. The whole atmosphere community climate model version 6 (WACCM6). *J. Geophys. Res.* **124**, 12380–12403 (2019).
18. Froidevaux, L. & Yung, Y. L. Radiation and chemistry in the stratosphere: Sensitivity to O₂ absorption cross sections in the Herzberg continuum. *Geophys. Res. Lett.* **9**, 854–857 (1982).
19. Mahieu, E. et al. Validation of ACE-FTS v2.2 measurements of HCl, HF, CCl₃F and CCl₂F₂ using space-, balloon- and ground-based instrument observations. *Atmos. Chem. Phys.* **8**, 6199–6221 (2008).
20. Bernath, P. F. et al. Sixteen-year trends in atmospheric trace gases from orbit. *J. Quant. Spectrosc. Radiat. Transf.* **253**, 107178 (2020).
21. Brewer, A. W. Evidence for a world circulation provided by the measurements of helium and water vapour distribution in the stratosphere. *Q. J. R. Meteorol. Soc.* **75**, 351–363 (1949).
22. Dobson, G. M. B. Origin and distribution of the polyatomic molecules in the atmosphere. *Proc. R. Soc. Lond. A* **236**, 187–193 (1956).
23. Butchart, N. The Brewer–Dobson circulation. *Rev. Geophys.* **52**, 157–184 (2014).
24. Prinn, R. G. et al. History of chemically and radiatively important atmospheric gases from the Advanced Global Atmospheric Gases Experiment (AGAGE). *Earth Syst. Sci. Data* **10**, 985–1018 (2018).
25. Mahieu, E. et al. Recent Northern Hemisphere stratospheric HCl increase due to atmospheric circulation changes. *Nature* **515**, 104–107 (2014).
26. Harrison, J. J. et al. Satellite observations of stratospheric hydrogen fluoride and comparisons with SLIMCAT calculations. *Atmos. Chem. Phys.* **16**, 10501–10519 (2016).
27. Prather, M. J., Froidevaux, L. & Livesey, N. J. Observed changes in stratospheric circulation: decreasing lifetime of N₂O, 2005–2021. *Atmos. Chem. Phys.* **23**, 843–849 (2023).
28. Mote, P. W. et al. An atmospheric tape recorder: the imprint of tropical tropopause temperatures on stratospheric water vapor. *J. Geophys. Res.* **101**, 3989–4006 (1996).
29. Schoeberl, M. R. et al. Comparison of lower stratospheric tropical mean vertical velocities. *J. Geophys. Res.* **113**, D24109 (2008).
30. Linz, M. et al. The strength of the meridional overturning circulation of the stratosphere. *Nat. Geosci.* **10**, 663–667 (2017).
31. Butchart, N. et al. Multimodel climate and variability of the stratosphere. *J. Geophys. Res.* **116**, D05102 (2011).
32. Abalos, M. et al. The Brewer–Dobson circulation in CMIP6. *Atmos. Chem. Phys.* **21**, 13571–13591 (2021).
33. Garny, H. et al. Age of stratospheric air: progress on processes, observations, and long-term trends. *Rev. Geophys.* **62**, e2023RG000832 (2024).
34. Abalos, M., Randel, W. J. & Serrano, E. Variability in upwelling across the tropical tropopause and correlations with tracers in the lower stratosphere. *Atmos. Chem. Phys.* **12**, 11505–11517 (2012).
35. Rind, D. et al. Climate change and the middle atmosphere. Part I: the doubled CO₂ climate. *J. Atmos. Sci.* **47**, 475–494 (1990).
36. Butchart, N. et al. Simulations of anthropogenic change in the strength of the Brewer–Dobson circulation. *Clim. Dynam.* **27**, 727–741 (2006).
37. Hardiman, S. C., Butchart, N. & Calvo, N. The morphology of the Brewer–Dobson circulation and its response to climate change in CMIP5 simulations. *Q. J. R. Meteorol. Soc.* **140**, 1958–1965 (2014).
38. Engel, A. et al. Age of stratospheric air unchanged within uncertainties over the past 30 years. *Nat. Geosci.* **2**, 28–31 (2009).
39. Engel, A. et al. Mean age of stratospheric air derived from AirCore observations. *Atmos. Chem. Phys.* **17**, 6825–6838 (2017).
40. Butchart, N. & Scaife, A. Removal of chlorofluorocarbons by increased mass exchange between the stratosphere and troposphere in a changing climate. *Nature* **410**, 799–802 (2001).
41. Boone, C. D., Bernath, P. F. & Lecours, M. Version 5 retrievals for ACE-FTS and ACE-imagers. *J. Quant. Spectrosc. Radiat. Transf.* **310**, 108749 (2023).
42. Madronich, S. Photodissociation in the atmosphere: 1. Actinic flux and the effects of ground reflections and clouds. *J. Geophys. Res.* **92**, 9740–9752 (1987).
43. Madronich, S. & Weller, G. Numerical integration errors in calculated tropospheric photodissociation rate coefficients. *J. Atmos. Chem.* **10**, 289–300 (1990).
44. Ko, M. K. W., Sze, N. D. & Weisenstein, D. K. Use of satellite data to constrain the model-calculated atmospheric lifetime for N₂O: Implications for other trace gases. *J. Geophys. Res.* **96**, 7547–7552 (1991).
45. Prather, M. J. et al. Measuring and modeling the lifetime of nitrous oxide including its variability. *J. Geophys. Res.* **120**, 5693–5705 (2015).
46. Butchart, N. The stratosphere: a review of the dynamics and variability. *Weather Clim. Dynam.* **3**, 1237–1272 (2022).
47. Andrews, A. E. et al. Mean ages of stratospheric air derived from in situ observations of CO₂, CH₄, and N₂O. *J. Geophys. Res.* **106**, 32295–32314 (2001).
48. Polvani, L. M. et al. Significant weakening of Brewer–Dobson circulation trends over the 21st century as a consequence of the Montreal Protocol. *Geophys. Res. Lett.* **45**, 401–409 (2018).
49. Polvani, L. M. et al. Large impacts, past and future, of ozone-depleting substances on Brewer–Dobson circulation trends: a multimodel assessment. *J. Geophys. Res.* **124**, 6669–6680 (2019).
50. Fu, Q. et al. Observed changes in Brewer–Dobson circulation for 1980–2018. *Environ. Res. Lett.* **14**, 114026 (2019).
51. Daniel, J. S. et al. Present and future sources and emissions of halocarbons: toward new constraints. *J. Geophys. Res.* **112**, D02301 (2007).
52. Laube, J. C. et al. Chapter 1: Update on ozone-depleting substances (ODSs) and other gases of interest to the Montreal Protocol. In: Scientific Assessment of Ozone Depletion: 2022 (World Meteorological Organization, 2023).
53. Hall, T. M. & Plumb, R. A. Age as a diagnostic of stratospheric transport. *J. Geophys. Res.* **99**, 1059–1070 (1994).
54. Lickley, M. et al. Joint inference of CFC lifetimes and banks suggests previously unidentified emissions. *Nat. Commun.* **12**, 2920 (2021).
55. Sparling, L. C. et al. Diabatic cross-isentropic dispersion in the lower stratosphere. *J. Geophys. Res.* **102**, 25817–25829 (1997).

56. Hersbach, H. et al. The ERA5 global reanalysis. *Q. J. R. Meteorol. Soc.* **146**, 1999–2049 (2020).
 57. Harrison, J. J. New and improved infrared absorption cross sections for trichlorofluoromethane (CFC-11). *Atmos. Meas. Tech.* **11**, 5827–5836 (2018).
 58. Harrison, J. J. New and improved infrared absorption cross sections for dichlorodifluoromethane (CFC-12). *Atmos. Meas. Tech.* **8**, 3197–3207 (2015).
 59. Harrison, J. J., Boone, C. D. & Bernath, P. F. New and improved infra-red absorption cross sections and ACE-FTS retrievals of carbon tetrachloride (CCl₄). *J. Quant. Spectrosc. Radiat. Transf.* **186**, 139–149 (2017).
 60. Linz, M. et al. The relationship between age of air and the diabatic circulation of the stratosphere. *J. Atmos. Sci.* **73**, 4507–4518 (2016).
 61. Gelaro, R. et al. The modern-era retrospective analysis for research and applications, version 2 (MERRA-2). *J. Clim.* **30**, 5419–5454 (2017).
 62. Rosenlof, K. H. Seasonal cycle of the residual mean meridional circulation in the stratosphere. *J. Geophys. Res.* **100**, 5173–5191 (1995).
 63. Randel, W. J., Wu, F., Russell, J. M., Roche, A. & Waters, J. W. Seasonal cycles and QBO variations in stratospheric CH₄ and H₂O observed in UARS HALOE data. *J. Atmos. Sci.* **55**, 163–185 (1998).
 64. Plumb, R. A. Tracer interrelationships in the stratosphere. *Rev. Geophys.* **45**, RG4005 (2007).
 65. Schmidt, M., Bernath, P., Boone, C., Lecours, M. & Steffen, J. Trends in atmospheric composition between 2004–2023 using version 5 ACE-FTS data. *J. Quant. Spectrosc. Radiat. Transf.* **325**, 109088 (2024).
 66. Froidevaux, L., Kinnison, D. E., Wang, R., Anderson, J. & Fuller, R. A. Evaluation of CESM1 (WACCM) free-running and specified dynamics atmospheric composition simulations using global multispecies satellite data records. *Atmos. Chem. Phys.* **19**, 4783–4821 (2019).
 67. Schwartz, M., Froidevaux, L., Livesey, N., Read, W. & Fuller, R. MLS/Aura Level 3 Monthly Binned Ozone (O₃) Mixing Ratio on Assorted Grids V005, Greenbelt, MD, USA, Goddard Earth Sciences Data and Information Services Center (GES DISC) [Data set]. <https://doi.org/10.5067/Aura/MLS/DATA/3546> (last access: February 25, 2025) (2021).
 68. Sheese, P. E. et al. Assessment of the quality of ACE-FTS stratospheric ozone data. *Atmos. Meas. Tech.* **15**, 1233–1249 (2022).
 69. Bourguet, S. Code and data for Semi-empirical estimates of stratospheric circulation and the lifetimes of chlorofluorocarbons and carbon tetrachloride [Data set]. Zenodo. <https://doi.org/10.5281/zenodo.15652978> (last access: June 12, 2025) (2025).
 70. Suntharalingam, P. et al. Evaluating oceanic uptake of atmospheric CCl₄: a combined analysis of model simulations and observations. *Geophys. Res. Lett.* **46**, 472–482 (2019).
 71. Rhew, R. C. & Happell, J. D. The atmospheric partial lifetime of carbon tetrachloride with respect to the global soil sink. *Geophys. Res. Lett.* **43**, 2889–2895 (2016).
- Tacolneston are funded by DESNZ. Financial support for the AGAGE measurements at Jungfraujoch is provided by the Swiss National Programs HALCLIM and CLIMGAS-CH (Swiss Federal Office for the Environment) and by the International Foundation High Altitude Research Stations Jungfraujoch and Gornegrat. AGAGE operations at Trinidad Head are funded by NASA in the USA. AGAGE operations at Ragged Point are currently supported by NASA Grant 80NSSC21K1369 (to MIT, under sub-award S5608 to the University of Bristol) with additional funding from the National Oceanic and Atmospheric Administration (NOAA) Contract 1305M319CNRMJ0028 (to the University of Bristol). Operation of the American Samoa Observatory (SMO) is funded by NOAA in the USA. AGAGE operations at SMO are funded by NASA in the USA. The Kennaoak/Cape Grim station is funded and managed by the Australian Bureau of Meteorology, with the AGAGE scientific program jointly managed with the Commonwealth Scientific and Industrial Research Organization (CSIRO). Support is also received from the Australian Department of Climate Change, Energy, the Environment and Water, Refrigerant Reclaim Australia, and through the NASA Upper Atmospheric Research Program award to MIT (80NSSC21K1369) with a sub-award to CSIRO for Kennaoak/Cape Grim AGAGE activities.

Author contributions

S.B. and M.L. conceptualized the study. S.B. developed the methods, obtained and analyzed data, and drafted the manuscript. K.S. performed N₂O loss rate calculations. S.B., K.S., and M.L. contributed revisions to the manuscript.

Competing interests

The authors declare no competing interests.

Additional information

Supplementary information The online version contains supplementary material available at <https://doi.org/10.1038/s43247-025-02500-0>.

Correspondence and requests for materials should be addressed to Stephen Bourguet.

Peer review information *Communications Earth & Environment* thanks Jing Wu and the other, anonymous, reviewer(s) for their contribution to the peer review of this work. Primary Handling Editors: Mengze Li and Alice Drinkwater. A peer review file is available.

Reprints and permissions information is available at <http://www.nature.com/reprints>

Publisher's note Springer Nature remains neutral with regard to jurisdictional claims in published maps and institutional affiliations.

Acknowledgements

The authors would like to acknowledge support from the VoLo Foundation and from the Atmospheric Chemistry Division of the National Science Foundation (grant no. 2128617, M.L. and K.S.). The authors thank Doug Kinnison for providing WACCM6 and WACCM-SD output, Luke Western for providing CFC-11, CFC-12, and CCl₄ emissions estimates from the 2022 Scientific Assessment of Ozone Depletion, and Chris Boone for helpful insights regarding ACE-FTS measurements. The authors acknowledge Susan Solomon for useful discussions. AGAGE is supported principally by the National Aeronautics and Space Administration (NASA; USA) grants to the Massachusetts Institute of Technology (MIT) and the Scripps Institution of Oceanography. The halocarbon measurements at Zeppelin Observatory are funded by the Norwegian Environment Agency. Atmospheric gas measurements at Mace Head are supported by research grants from the Department of Energy, Security and Net Zero (DESNZ), contract number 5488/11/2021 in the UK; and NASA, sub-award S5608 PO#—752393. Atmospheric gas measurements at

Open Access This article is licensed under a Creative Commons Attribution 4.0 International License, which permits use, sharing, adaptation, distribution and reproduction in any medium or format, as long as you give appropriate credit to the original author(s) and the source, provide a link to the Creative Commons licence, and indicate if changes were made. The images or other third party material in this article are included in the article's Creative Commons licence, unless indicated otherwise in a credit line to the material. If material is not included in the article's Creative Commons licence and your intended use is not permitted by statutory regulation or exceeds the permitted use, you will need to obtain permission directly from the copyright holder. To view a copy of this licence, visit <http://creativecommons.org/licenses/by/4.0/>.

© The Author(s) 2025